Supplementary Figure 1

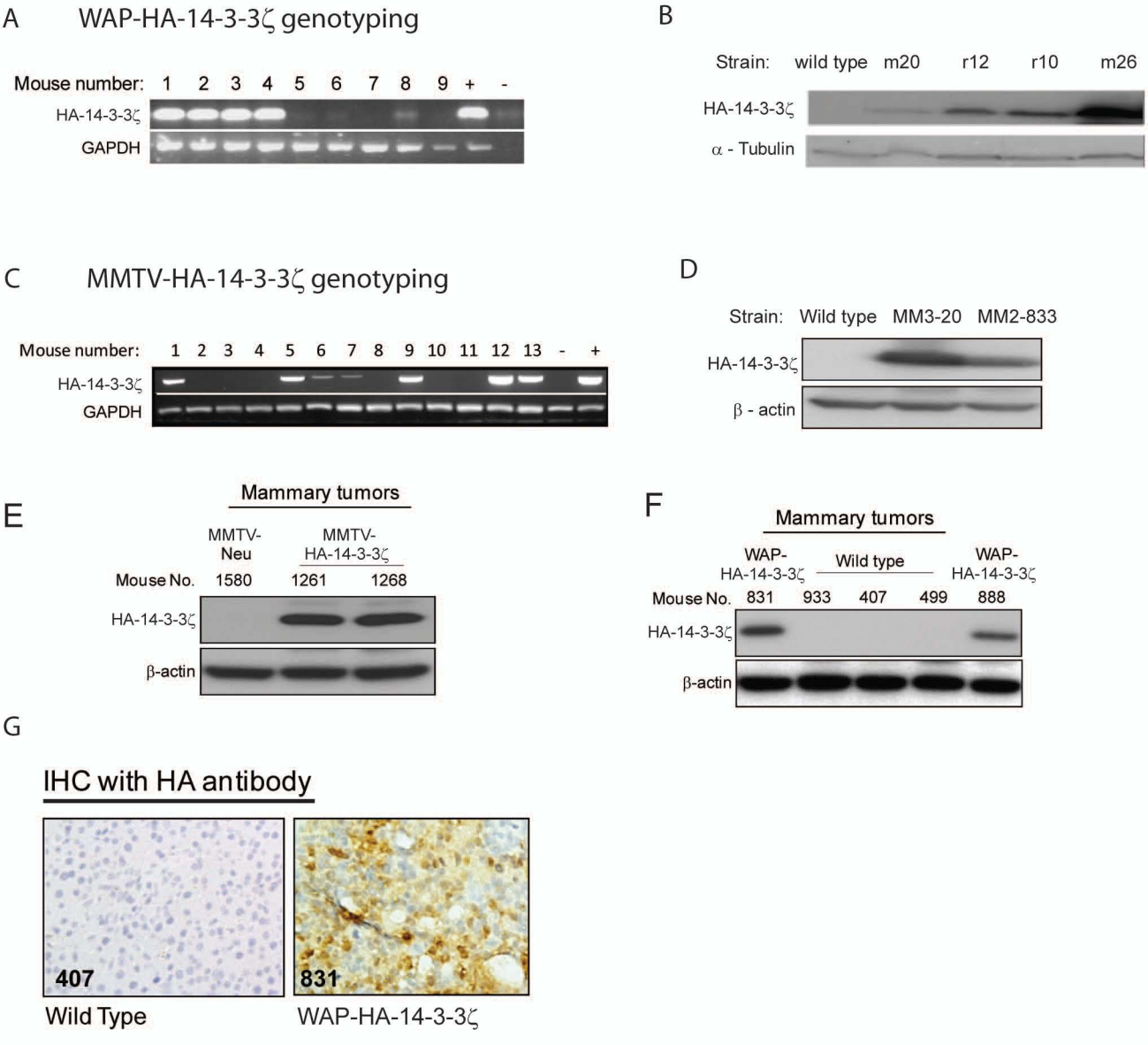

Supplementary Figure 1: Characterization of 14-3-3ζ Transgenic Mice and Mammary Tumors. *A,B,* Representative PCR screening of WAP-HA-14-3-3ζ transgenic founder mice and IB detection of HA-14-3-3ζ protein expression in mammary glands of WAP-HA-14-3-3ζ transgenic mice strains. *C,D,* Representative PCR screening of MMTV-HA-14-3-3ζ transgenic founder mice and IB detection of HA-14-3-3ζ protein expression in mammary glands of MMTV-HA-14-3-3ζ transgenic mice strains. *E,* IB of HA-14-3-3ζ protein expression in mammary tumors of MMTV-HA-14-3-3ζ mice. MMTV-*neu* mouse mammary tumor serves as a negative control. *F,* IB and *G,* IHC of HA-14-3-3ζ expression (400x magnification) in mammary tumors from DMBA-treated WAP-HA-14-3-3ζ transgenic and wild-type mice.

Supplementary Figure 2

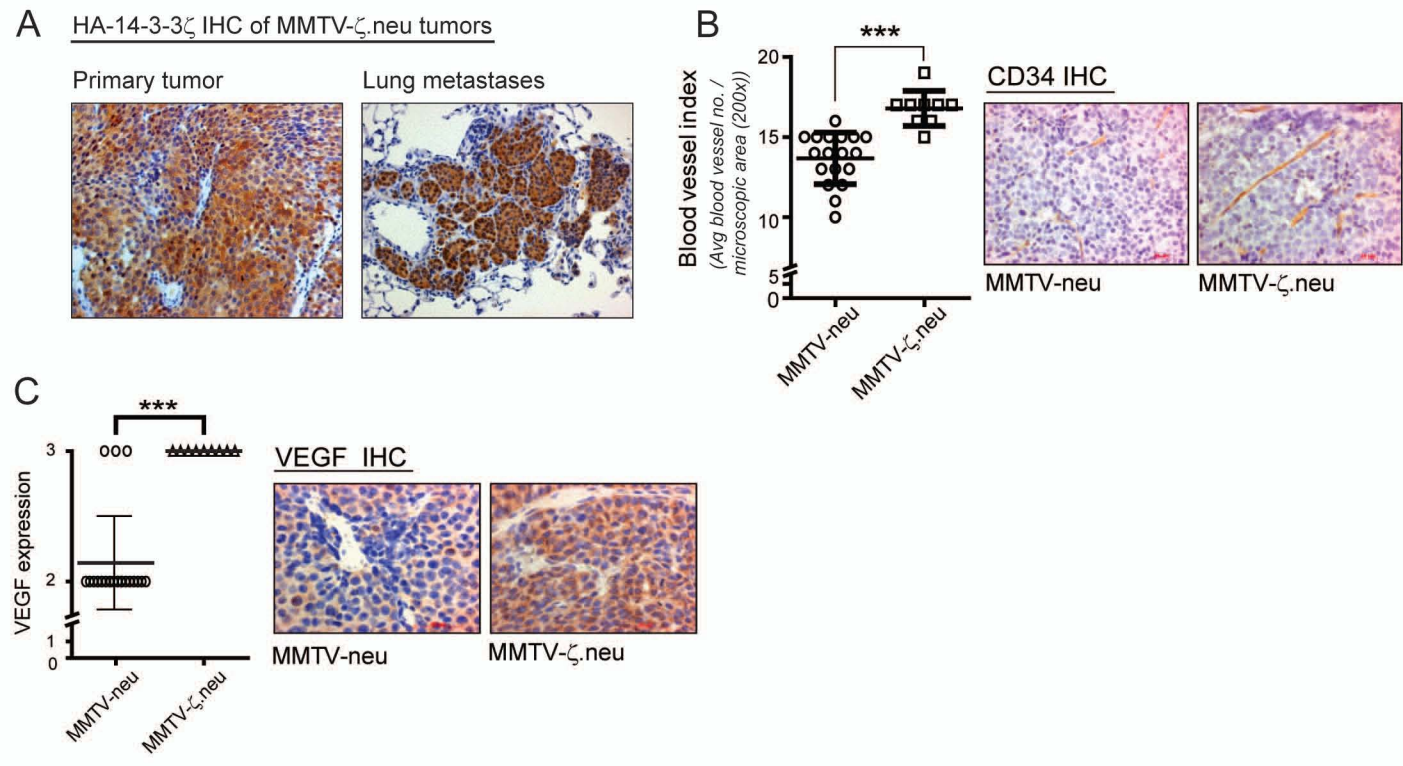

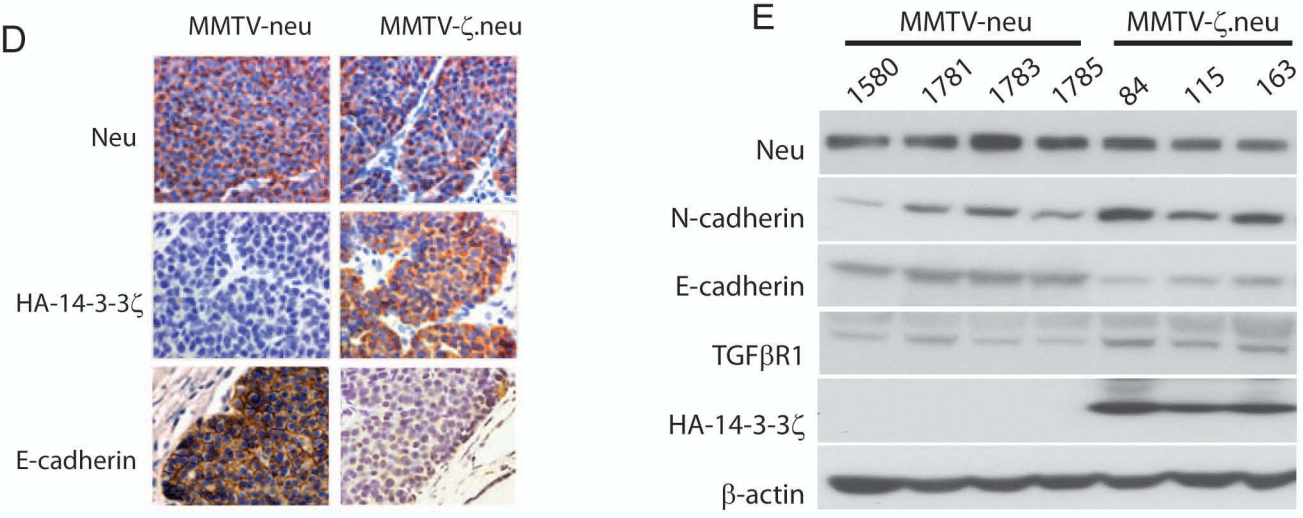

Supplementary Figure 2: Analysis of Metastasis in Mammary Tumors. *A,* Representative HA-14-3-3ζ IHC (X200) of matched primary tumor and lung metastases that originated from the HA-14-3-3ζ overexpressing tumors. *B,* Average blood vessel index (left) is higher in mammary tumors from MMTV-ζ.*neu* (n=9) mice than MMTV-*neu* (n=18) mice. Representative CD34 IHC (right, X400). *C,* Quantitative analysis (left) and representative VEGF IHC (right, X400) showed increased expression in mammary tumors of MMTV-ζ.*neu* mice (n=9) versus MMTV-*neu* mice (n=21). *D,* Representative IHC of Neu, HA-14-3-3ζ and E-cadherin in mammary tumors of MMTV-*neu* and MMTV-ζ.*neu* mice (X400). *E,* IB of E-cadherin, N-cadherin and TGFβR1 in mammary tumors of MMTV-ζ.*neu* and MMTV-*neu* mice indicates EMT in 14-3-3ζ overexpressing tumors. Bars, SD. ***, *P< 0.001.*

Supplementary Figure 3

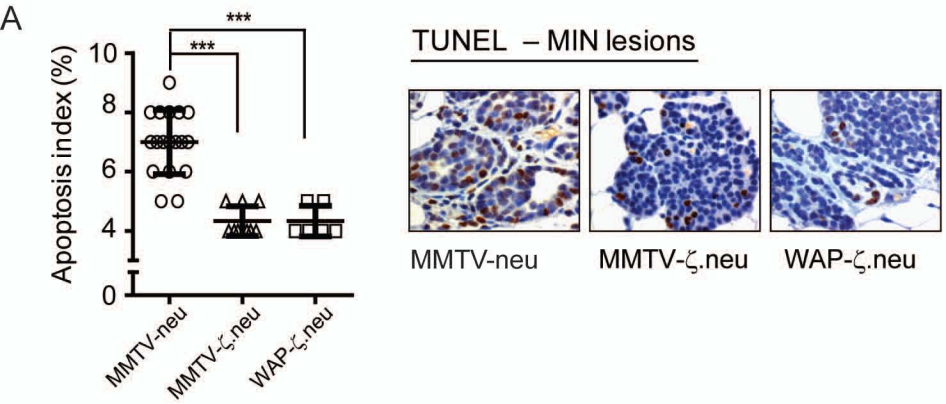

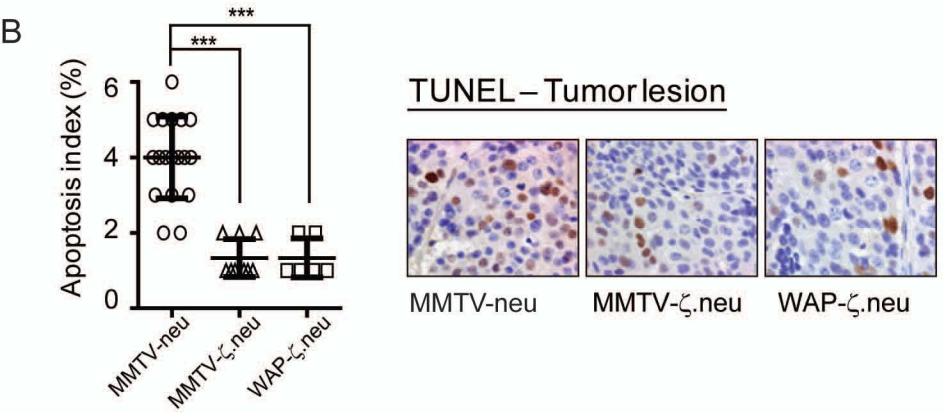

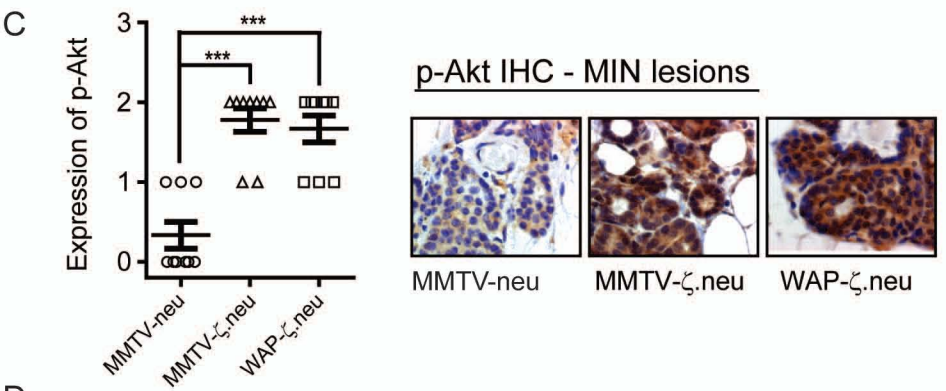

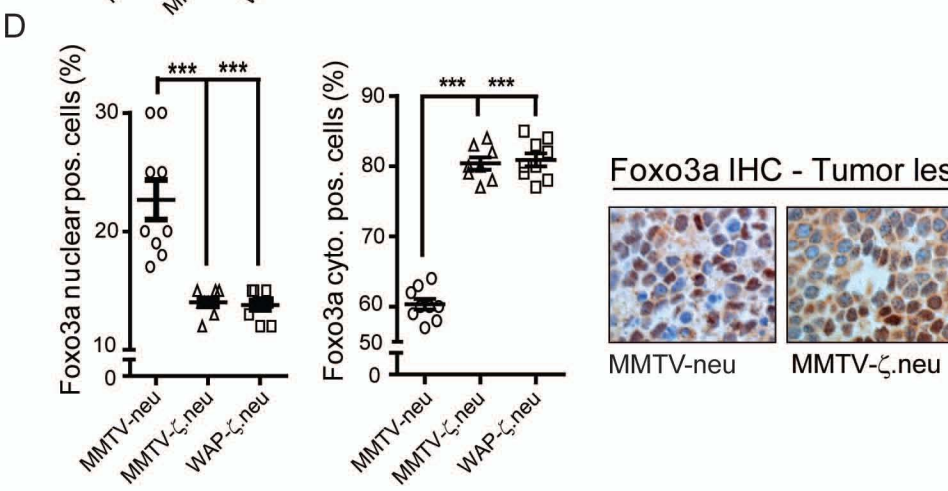

Supplementary Figure 3 - cont'd

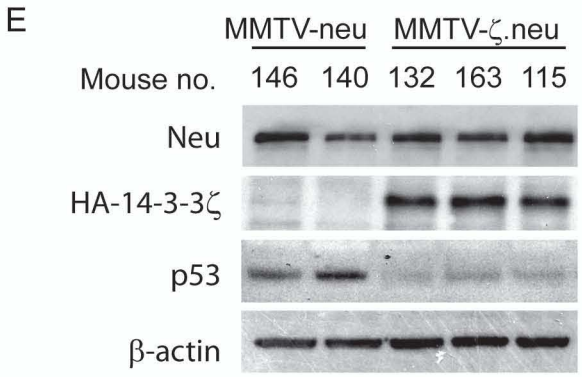

Supplementary Figure 3: Apoptosis Assays in Transgenic Mice and Cell Lines. *A,* Quantitative analysis (left) of the percentage of apoptotic cells by TUNEL assay and representative staining (right, X400) of MIN lesions showed significant (*P<0.001*) decrease in apoptosis in MMTV-ζ.*neu* and WAP-ζ.*neu* lesions compared to MMTV-*neu* lesions. Respectively, n=18, 9, 6. *B,* Quantitative analysis (left) of the percentage of apoptotic cells by TUNEL assay and representative staining (right, X400) in mammary tumors showed significant (*P<0.001*) decrease in apoptosis in MMTV-ζ.*neu* and WAP-ζ.*neu* tumors compared to MMTV-*neu* tumors. Respectively, n=18, 9, 6. *C,* Quantitative analysis (left) of p-Akt expression and representative IHC (right, X400) of MIN lesions showed significant (*P<0.001*) increase in expression in MMTV-ζ.*neu* and WAP-ζ.*neu* lesions compared to MMTV-*neu* lesions. All, n=9. *D,* Quantitative analysis of nuclear and cytoplasmic Foxo3a expression (left) and representative IHC of mammary tumors (right, X400) showed significant increase in cytoplasmic Foxo3a localization in MMTV-ζ.*neu* and WAP-ζ.*neu* tumors compared to MMTV-*neu* tumors (*P<0.001*). All groups, n=9. *E,* IB analysis of p53 expression shows p53 downregulation in MMTV-ζ.*neu* mammary tumors compared to MMTV-*neu* tumors. Bars, SD. ***, *P<0.001,* ****, *P<0.0001.*

Supplementary Figure 4

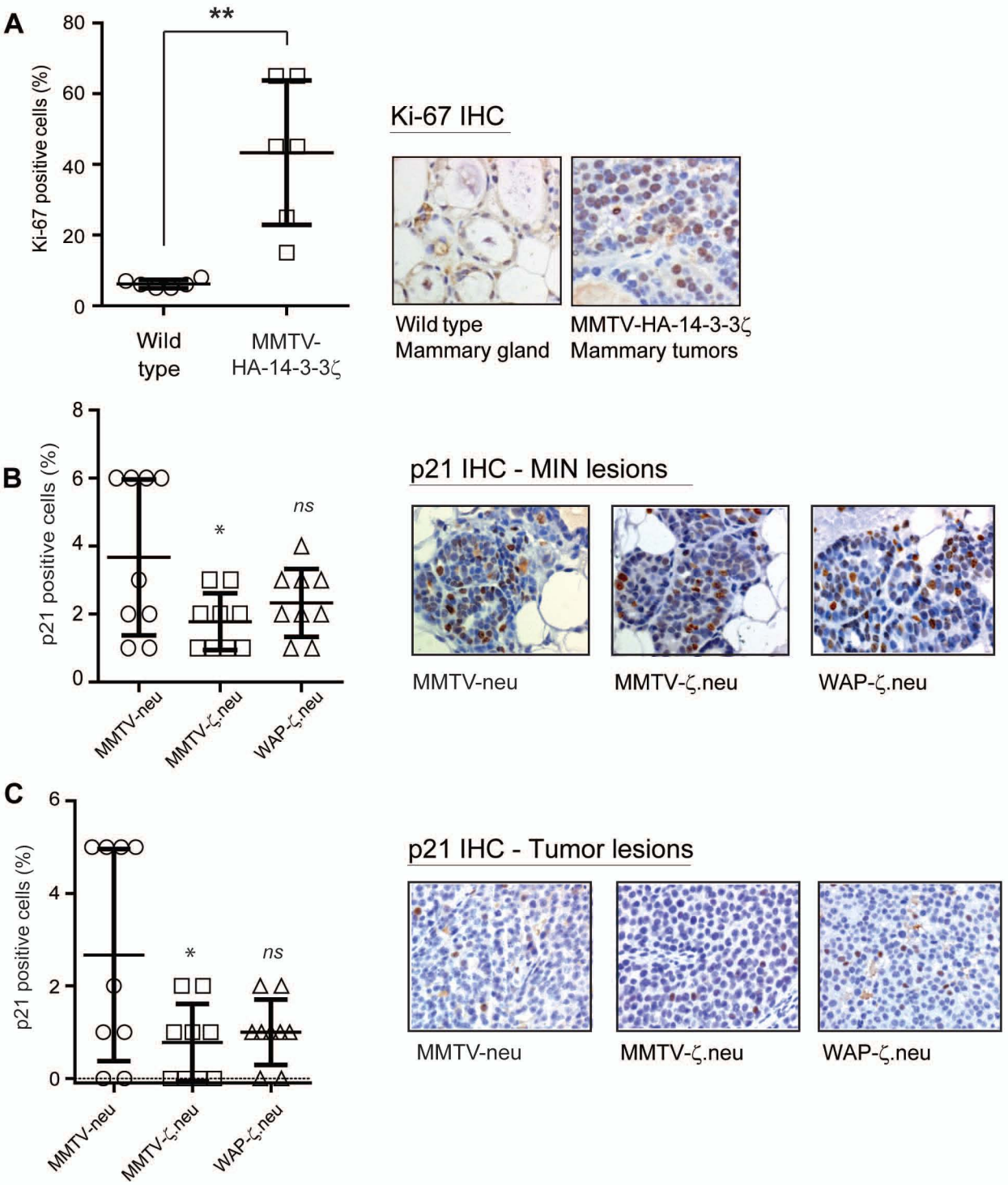

Supplementary Figure 4: IHC Staining of Ki-67 and p21 Expression. Quantitative analysis of Ki-67-positive nuclei (left) and representative IHC (right, X400) shows increased Ki-67 in MMTV-ζ.*neu* (*P=0.004*) mammary tumor lesions versus mammary gland of wildtype mice. Both, n=6. *B,C,* Quantitative analysis of p21 expression in MIN lesions and tumors of MMTV-ζ.*neu* and WAP-ζ.*neu* mice compared to MMTV-*neu* mice (left, all n-9) with representative p21 IHC (right, X400) showed a moderate decrease in the bitransgenic mice lesions. Bars, SD. **, *P< 0.01, *, P<0.05.*

Supplementary Figure 5

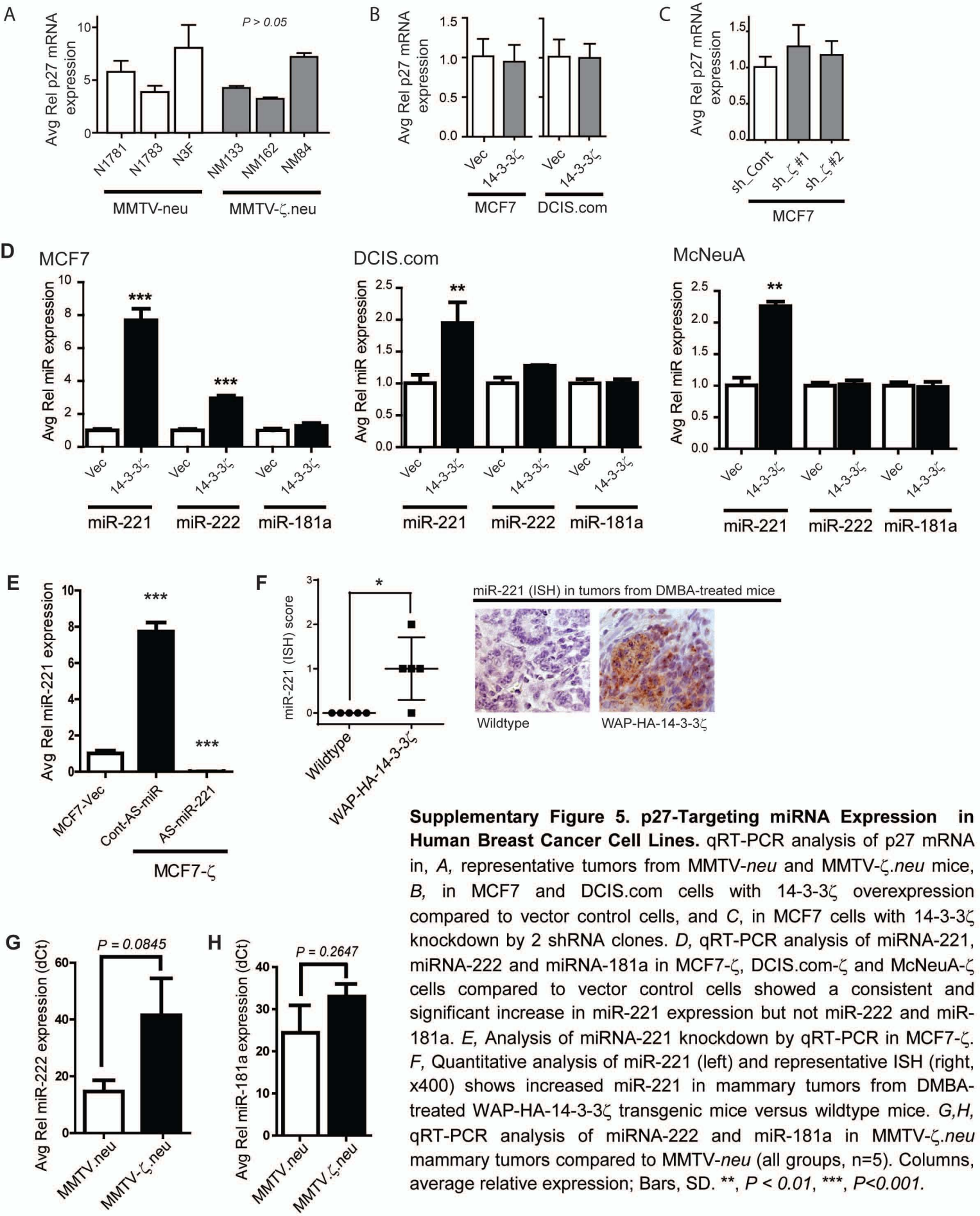

Supplementary Figure 5. p27-Targeting miRNA Expression in Human Breast Cancer Cell Lines. qRT-PCR analysis of p27 mRNA in, *A,* representative tumors from MMTV-*neu* and MMTV-ζ.*neu* mice, *B,* in MCF7 and DCIS.com cells with 14-3-3ζ overexpression compared to vector control cells, and *C*, in MCF7 cells with 14-3-3ζ knockdown by 2 shRNA clones. *D,* qRT-PCR analysis of miRNA-221, miRNA-222 and miRNA-181a in MCF7-ζ, DCIS.com-ζ and McNeuA-ζ cells compared to vector control cells showed a consistent and significant increase in miR-221 expression but not miR-222 and miR-181a. *E,* Analysis of miRNA-221 knockdown by qRT-PCR in MCF7-ζ. *F,* Quantitative analysis of miR-221 (left) and representative ISH (right, x400) shows increased miR-221 in mammary tumors from DMBA-treated WAP-HA-14-3-3ζ transgenic mice versus wildtype mice. *G,H,* qRT-PCR analysis of miRNA-222 and miR-181a in MMTV-ζ.*neu* mammary tumors compared to MMTV-*neu* (all groups, n=5). Columns, average relative expression; Bars, SD. **, $P < 0.01$, ***, $P<0.001$.

Supplemental Figure 6

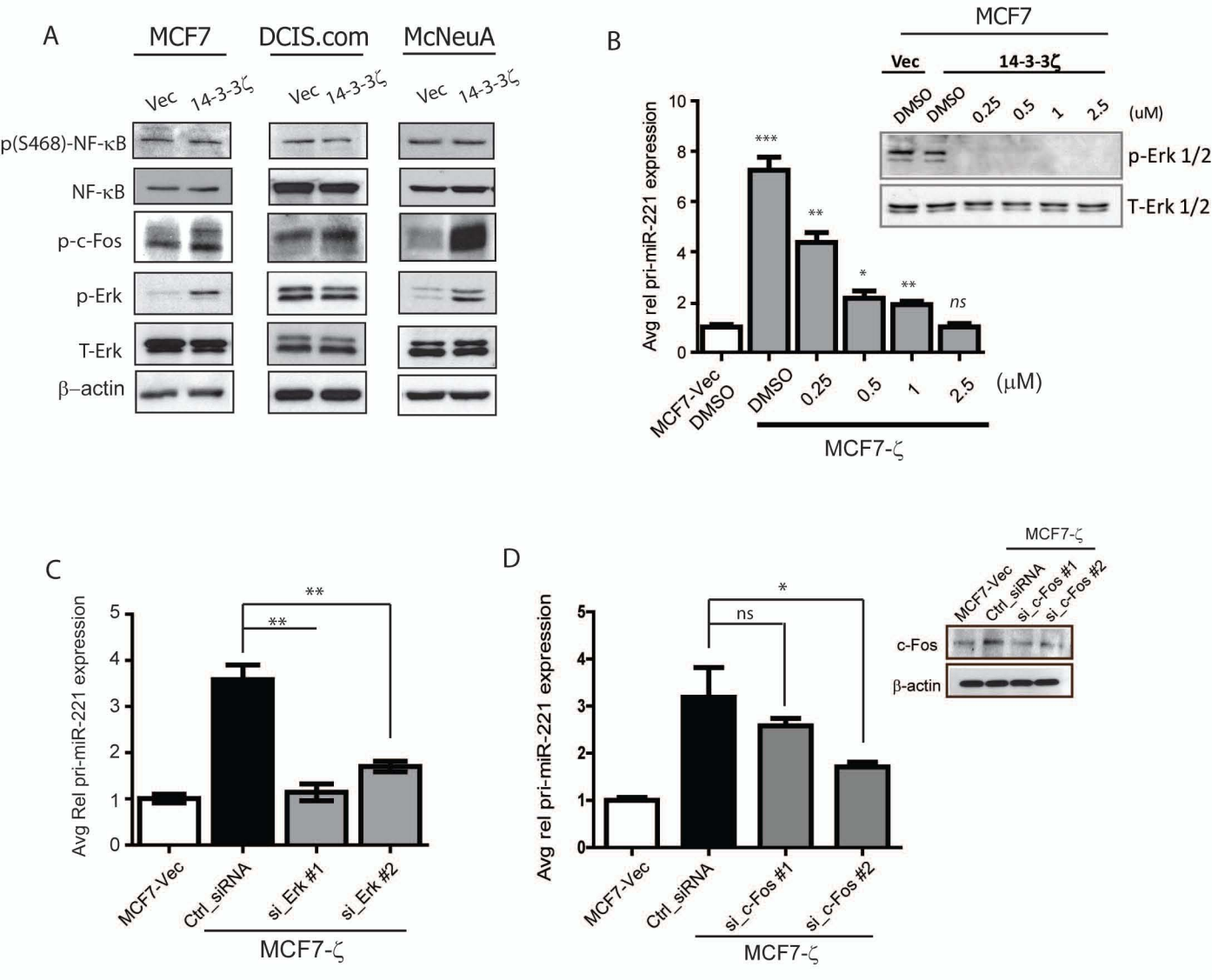

Supplementary Figure 6. Analysis of Signaling Pathways Involved in 14-3-3ζ-Mediated miR-221 Transcriptional Upregulation. *A,* IB analysis of NF-κB and c-Fos signaling pathways in MCF7-ζ, DCIS.com-ζ and McNeuA-ζ cells compared to vector control cells revealed that NF-κB is not significantly altered and c-Fos is differentially regulated between the cell lines. *B,* Erk1/2 inhibition in MCF7-ζ cells by AZD6244 significantly decreased pri-miR-221 expression in a dose-dependent manner after 24 hours of treatment, relative to vector cells treated with DMSO (IB inset, Erk1/2 expression). *C,* Erk1/2 inhibition by two different siRNA in MCF7-ζ cells decreased pri-miR-221 expression by qRT-PCR. *D,* qRT-PCR analysis decreased pri-miR-221 expression with c-Fos knockdown using two different siRNAs (IB inset) in MCF7. Bars, SD. *, *P<0.05,* **, *P < 0.01*, ***, *P<0.001.*

Supplementary Figure 7

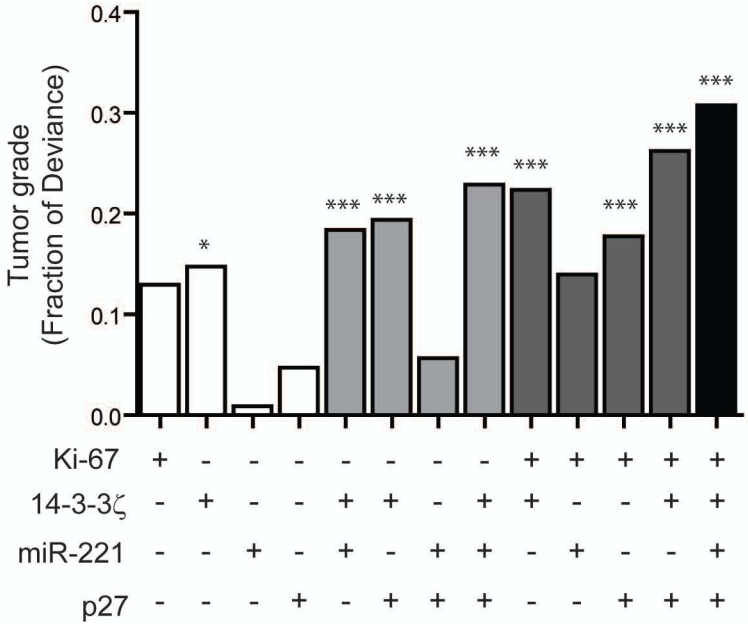

Supplementary Figure 7: Logistic regression model of 14-3-3ζ/miR-221/p27/Ki-67 axis to predict tumor grade as a fraction of deviance using single marker, varying marker combinations, or the linear combination of all markers of the 14-3-3ζ/miR-221/p27/Ki-67 axis.